Revista Ciência Agronômica, v. 56, e202292763, 2025
Centro de Ciências Agrárias - Universidade Federal do Ceará, Fortaleza, CE
www.ccarevista.ufc.br

Scientific Article
ISSN 1806-6690

Simulated performance of a tractor equipped with two types of tyre under two levels of soil moisture[1]

João Pedro Rodrigues da Silva[2]*, Cristiano Márcio Alves de Souza[3], Roberto Carlos Orlando[3], Jackson Antônio Barbosa[4], Tainara Regina Cerutti Torres Bahia[2]

ABSTRACT - Due to the importance of grain production, and the need to work the soil under limited moisture, the aim of this study was to develop computer software to predict the tractive capacity of wheeled tractors for two types of tyre, the effect of different inflation pressures and levels of soil moisture. A mathematical model was developed to predict the tractive capacity of a 4 x 2 AFT tractor. Software was developed and tested by comparing the computational data with those from tests of a working tractor in the field. The parameters under evaluation were drawbar force and front and rear drive wheel slip. At both moisture levels, the bias tyres had the lowest front to rear slip ratio at the lower pressure; the ratios were similar when equipped with radial tyres. The bias tyres show maximum force at a slip ratio of 1.09 at the higher pressure and 1.03 at the lower, while for the radial tyres the ratio was 1.05 at the higher pressure and 1.07 at the lower. Software was developed to process data from the model, with the results used for estimating the tractive force of the tractor. The tractive force was overestimated by the model, which needs further adjustment for direct application in the field.

Key words: Tractive efficiency. Agricultural mechanisation. Mathematical modelling.

DOI: 10.5935/1806-6690.20250022
Editor-in-Article: Prof. Daniel Albiero - daniel.albiero@gmail.com
*Author for correspondence
Received for publication on 26/09/2022; approved on 21/09/2023
[1]Part of the master's thesis of the main author, presented to the Federal University of Grande Dourados (UFGD)
[2]Postgraduate Program in Agricultural Engineering (UFGD), highway Dourados-Itahum, km 12, Dourados-MS, Brazil, joaopedro_rodrigues@hotmail.com (ORCID ID 0000-0003-0630-7786), tainara_cerutti@hotmail.com (ORCID ID 0009-0009-9973-1252)
[3]Faculty of Agricultural Sciences (UFGD), Dourados-MS, Brazil, csouza@ufgd.edu.br (ORCID ID 0000-0002-5347-1709), robertoorlando@ufgd.edu.br (ORCID ID 0000-0003-4802-7803)
[4]Departament of Agricultural Engineering, Federal University of Lavras (UFLA), Lavras-MG, Brazil, jackson@ufla.br (ORCID ID 0009-0008-5772-7653)

INTRODUCTION

Agriculture is important to the development of the Brazilian economy because of its versatility and the economic returns it affords producers and companies. In addition, there is a need to provide food for the growing population. However, the challenges facing agricultural production are great, involving the sustainability of cultivated areas and meeting food requirements.

For Pinho, Cunha and Morais (2015), public concern about environmental issues and more efficient management of production processes have led to the development of a new agricultural concept, known as precision agriculture, which for Aubert, Schroeder and Grimaudo (2012) combined the use of information technology to assist decision-making processes in order to reduce risks that affect productivity and operational costs while maintaining high efficiency. This makes it possible to reduce and optimise the use of potentially harmful components, minimising their impact on the environment (Zhang; Seelan; Seielstad, 2010; Zhang; Kovacs, 2012).

In modern agriculture, man has increasingly implemented new technology, seeking to increase productivity and reduce costs, thereby obtaining greater profit per unit area. Machines and implements available for agricultural mechanisation have high technology built-in, and tools that, when used correctly, can afford increasing efficiency in field operations (Almeida; Tavares-Silva; Silva, 2010). Today, this new technology is reaching a larger number of producers.

The study of agricultural operations should take into account work capacity and operational efficiency (Souza *et al.*, 2022a), the optimisation of machine traffic and product transportation (Pron *et al.*, 2020), and intelligent tools as an aid to carrying out the work (Hart; Quendler; Umstaetter, 2022). It is therefore important to determine the behaviour of machines in operation, looking at such details as fuel consumption, operating speed, and working width.

Borges *et al*. (2017) and Araujo *et al*. (2022) show that in the search for the best performance of a tractor in different work situations, mathematical modelling can describe the operational behaviour of agricultural machines in the field, accurately characterising the interaction between the wheels and the ground and, as a result, the tractive efficiency and performance of the tractor.

With the digital or technological age, countless computer programs have been created, including software to analyse the tractive capacity of agricultural tractors using mathematical models. The aim of this study was to develop computer software to predict the tractive capacity of wheeled tractors, and test it for two types of tyre, two inflation pressures and two levels of soil moisture.

MATERIAL AND METHODS

Tractor modelling

Modelling the tractive capacity of the tractor with both types of tyre was carried out as per the method proposed by Goering *et al*. (2003) and the D497.5 standard (Asabe, 2006a).

The dynamic loads on the front and rear wheels were calculated using force moment balance, considering the turning point to be the contact between the rear tyre and the ground. The dynamic loads were calculated using Equations 1 and 2.

$$R_f = \frac{W_t \cos(\beta) x_1 - W_t \sin(\beta) z_1 - P \sin(\alpha) x_3 - p \cos(\alpha) z_3 - TF_f r_f - TF_r r_r}{x_1 + x_2} \quad (1)$$

$$R_r = W_t \cos(\beta) + P \sin(\alpha) - R_f \quad (2)$$

where: TF_f - front tyre rolling resistance force, kN; TF_r - rear tyre rolling resistance force, kN; R_f - front wheel dynamic load applied to the ground, kN; R_r - rear wheel dynamic load applied to the ground, kN; W_t - total weight of the tractor, kN; P - drawbar force, kN; r_f - front tyre rolling radius, m; r_r - rear tyre rolling radius, m; x_1 - distance between the rear axle and the centre of gravity of the tractor projected onto the x-axis, m; z_1 - distance between the ground and the centre of gravity of the tractor projected onto the z-axis, m; x_2 - distance between the front axle and the centre of gravity of the tractor projected onto the x-axis, m; x_3 - distance between the rear axle and the point of application of the drawbar force projected onto the x-axis, m; z_3 - distance between the ground and the point of application of the drawbar force projected onto the z-axis, m; β - slope of the terrain, rad; α - angle of application of force P relative to the x-axis, rad.

The forces from rolling resistance were calculated using Equations 3 and 4 (Asabe, 2006a). Dimensions x_1, z_1, x_2, x_3 and z_3 were calculated using Equations 5 to 9.

$$TF_f = R_f \left[\frac{C_3}{B_{nf}} + C_2 + \frac{0.5 s_f}{\sqrt{B_{nf}}} \right] \quad (3)$$

$$TF_r = R_r \left[\frac{C_3}{B_{nr}} + C_2 + \frac{0.5 s_r}{\sqrt{B_{nr}}} \right] \quad (4)$$

$$x_1 = h_{1t} \cos(\theta_{1t}) \quad (5)$$

$$Z_1 = r_r + h_{1t} \sin(\theta_{1t}) \quad (6)$$

$$x_2 = h_{2t} \cos(\theta_{2t}) \quad (7)$$

$$x_3 = h_3 \sin(\theta) \quad (8)$$

$$Z_3 = r_r - h_3 \cos(\theta) \quad (9)$$

where: B_{nf} - mobility coefficient of the front tyres, dimensionless; B_{nr} - mobility coefficient of the rear tyres,

dimensionless; s_f - front wheel slip, dec.; s_r - rear wheel slip, dec.; C2, C3 - coefficients that depend on the type of tyre, as per Table 1; h_{1t} - distance between the centre of gravity of the tractor and the centre of the rear wheel, m; Θ_{1t} - angle between the x-axis and the line joining the centre of the rear wheel and the centre of gravity of the tractor, rad.; h_{2t} - distance between the centre of gravity of the tractor and the centre of the front wheel rim, m; Θ_{2t} - angle between the x-axis and the line segment joining the centre of the front wheel rim and the centre of gravity of the tractor, rad.; h_3 - distance between the centre of the rear wheel and the point of application of force *P*, m; Ø - angle between the z-axis and the line segment joining the centre of the rear wheel and the point of application of force *P*, rad.

The available drawbar force is determined from the difference between the gross tractive force, the rolling resistance and the weight force component of the tractor, as per Equation 10. The front and rear gross tractive forces were calculated using Equations 11 and 12, respectively. While the mobility coefficients of the tyres were determined using Equations 13 and 14. An adjustment factor K was adopted in the model, since the model coefficients of the D497.5 standard (Asabe, 2006a) may not properly represent the tyre-ground interaction under the extreme conditions tested in the study.

$$F_f - TF_f + F_r - TF_t - W_t sen(\beta) - P\cos(\alpha) = 0 \quad (10)$$

$$F_f = R_f\left[K\,0.88\left(1-e^{-0.1B_{nf}}\right)\left(1-e^{-C1s_f}\right)+C_2\right] \quad (11)$$

$$F_r = R_r\left[K\,0.88\left(1-e^{-0.1B_{nr}}\right)\left(1-e^{-C_1Sr}\right)+C_2\right] \quad (12)$$

$$B_{nf} = \left(\frac{I_{C0}b_f d_f}{\frac{R_f}{2}}\right)\left(\frac{1+5\frac{\delta_f}{h_f}}{1+3\frac{b_f}{d_f}}\right) \quad (13)$$

$$B_{nr} = \left(\frac{I_{C1}b_r d_r}{\frac{R_r}{2}}\right)\left(\frac{1+5\frac{\delta_r}{h_r}}{1+3\frac{b_r}{d_r}}\right) \quad (14)$$

where: F_f - gross tractive force available on the front tyre, kN; F_r - gross tractive force available on the rear tyre, kN; *C*1, *C*2 - constants that depend on the type of tyre, as per Table 1; I_{C0} - soil cone index before passage of the front tyre, kPa; I_{C1} - soil cone index before passage of the rear tyre, kPa; *b* - tyre tread width, where *f* - front and *r* - rear, m; *d* - tyre diameter, where *f* - front and *r* - rear, m; *h* - tyre tread height, where *f* - front and *r* - rear, m; *K* - adjustment factor, dimensionless; δ - tyre deflection, where *f* - front and *r* - rear, m.

Table 1 - Coefficients that characterise the performance of radial and bias tyres

Coefficients	Radial tyre	Bias tyre
C1	9.5	7.5
C2	0.032	0.040
C3	0.9	1.0

Source: Brixius (1987)

The ratio between the front and rear wheel slip was determined using Equation 15. Equations 16 and 17 show the deflections of the front and rear tyres, respectively.

$$S_f = 1-\left[\frac{r_r G_f}{r_f G_r}(1-S_r)\right] = \lambda s_r \quad (15)$$

$$\delta_f = \frac{d_f}{2} - r_{ef} \quad (16)$$

$$\delta_r = \frac{d_r}{2} - r_{er} \quad (17)$$

where: λ - ratio between the front and rear wheel slip, measured directly in the field, adm.; G_f - transmission ratio between the engine and the front wheel, adm.; G_r - transmission ratio between the engine and the rear wheel, adm.; r_{ef} - static radius of the front tyre on a firm surface, m; r_{er} - static radius of the rear tyre on a firm surface, m.

The effective torque developed at the front and rear wheel axles was calculated using Equations 18 and 19. Tractive efficiency, defined as the ratio between the drawbar force and force on the drive axle, was calculated using Equation 20. The available drawbar power of the tractor was determined using Equation 21.

$$T_{wf} = F_f r_f \quad (18)$$

$$T_{wr} = F_r r_r \quad (19)$$

$$E_T = \frac{Hp_b}{Hp_{axle}} = \frac{P}{\frac{F_f}{1-S_f}+\frac{F_r}{1-s_r}} \quad (20)$$

$$Hp_b = Pv \quad (21)$$

where: T_{wf} - torque on the front wheel axle, Nm; T_{wr} - torque on the rear wheel axle, Nm; E_T - tractive efficiency, dec.; Hp_b - net tractive drawbar force, kW; Hp_{axle} - force available at the wheel axle, kW; *v* - tractor ground speed, m s^{-1}.

The maximum power available at the wheel axle of the tractor was calculated using Equation 22. Due to the partial acceleration, the engine power usage index resulted in a lower rotation than at maximum power. The engine power index, again due to the use of partial acceleration, was determined using Equation 23.

$$Hp_{axle} = Hp_e n_1 n_2 i_{ep} \quad (22)$$

$$i_{ep} = \frac{T_1\omega_1}{T_2\omega_2} \quad (23)$$

where: Hp_e - engine power, kW; η_1 - transmission efficiency between the engine and the PTO at the applied engine acceleration, dec.; η_2 - transmission efficiency between the PTO and the wheel axle, dec.; i_{ep} - engine power generation index due to partial acceleration, dec.; T_1 - torque at partial engine acceleration, Nm; T_2 - acceleration torque at the rated engine power, Nm; ω_1 - rotation at partial engine acceleration, rpm; ω_2 - acceleration rotation at the rated engine power, rpm.

To carry out the model calculations, an algorithm was implemented, and a software was developed using the Excel™ VBA application (Chamon, 2019). With this software, it is possible to calculate the following data of interest: drawbar force, front and rear wheel slip, tractor speed, torque at the hub of the drive wheels and the engine, and tractive efficiency.

The idea behind the programme is to start with a known or estimated drawbar force, for example, the force needed to pull an implement or machine. In this case, all that's needed in the field is to start the tractor and measure the slip of both wheels, which is not difficult to do. From there, the force is increased until the rear wheel slip exceeds 35%, the maximum power on the PTO of the tractor is reached, or the weight transfer to the rear axle exceeds 80% of the weight at the front.

The developed software presents seven spreadsheets for data entry and execution of the calculation procedures: Soils - to characterise the terrain; Tractor - for character weighting and to input the operational parameters; Tyres - to specify the wheels; Prediction – for data entry, with buttons for execution and control; Results - shows the calculated data in the form of editable tables; Graphs - shows the behaviour of the variables of interest. Test data, such as those used to test the program, can be entered into the Test spreadsheet and compared to the results.

Field tests

The field tests were conducted in an area of soil classified as a dystrophic Red-Yellow Argisol (Santos *et al*., 2018) with a very clayey texture, located between 20°44'41" S and 42°50'31" W, at an altitude of 650 m. The soil had a density of 1.32 Mg m^{-3}, a clay content of 0.68, sand content of 0.15, and silt content of 0.17 kg kg^{-1}.

Only Pirelli tyres were used in the tests: model TM-95 with diagonal casing, size 18.4-32PR10 at the rear and TM-95 size 14.9-24PR8 at the front; or model TM-700 with radial casing, size 510/70R32PR8 at the rear and TM-200 size 14.9R24PR8 at the front. The characteristics of the tyres are shown in Table 2.

A model MF5290 4x2 tractor with auxiliary front wheel drive was used in the tests. The tractor has a maximum engine power of 77 kW (105 hp) at 2,200 rpm, engine transmission efficiency and PTO of 0.84 (540 rpm at the PTO), and transmission efficiency from the PTO to the wheel hub shaft of 0.94 (Asabe, 2006a). The total weight of the tractor was 37.36 kN when equipped with radial tyres and 38.18 kN when equipped with bias tyres, with a static weight distribution of 42.7% and 57.3%, respectively, for front and rear axles 2286 mm apart.

The drawbar forces of the MF5290 tractor were generated by a braking tractor with an 81-kW engine and a ballasted weight of 6.8 Mg.

The field tests employed univariate analysis in a completely randomised design (Favero; Belfiore, 2017) to test two types of tyre construction (bias and radial), two levels of soil moisture, and two inflation settings (high and low pressure) for each type of tyre (Table 3). Also tested were 14 different drawbar loads, generating 14 sets of tyre-slip data caused by the braking tractor.

The tractor was tested under two conditions of extreme soil moisture, one corresponding to 'planting in the dust' (0.06 m^3 m^{-3}), a term used in situations where it is necessary to bring sowing forward in the Cerrado region, or during a period of prolonged drought within the zoning area in expectation of the rain promised for a few days after the operation, and when allowed by the type of soil management. The tests were repeated using the same treatments, but

Table 2 - Characteristics of the tyres used in the tests

Wheelset	Model	Specification	Width (m)	Diameter (m)	Section height (m)	Rolling radius (m)	δ (m)
Low pressure							
Front	TM-95	14.9-24	378.5	1253.1	321.7	626.5	19.0
Back	TM-95	18.4-32	467.4	1658.2	422.7	829.1	48.8
Front	TM-200	14.9R24	378.5	1139.5	265.0	569.8	10.0
Back	TM-700	520/70R32	520.0	1591.6	389.4	795.8	25.4
High pressure							
Front	TM-95	14.9-24	378.5	1204.9	297.6	602.4	60.5
Back	TM-95	18.4-32	467.4	1594.4	390.8	797.2	58.0
Front	TM-200	14.9R24	378.5	1089.2	239.8	544.6	18.0
Back	TM-700	520/70R32	520.0	1512.9	350.1	756.5	40.0

under less moisture than the limiting moisture (0.51 $m^3 m^{-3}$) for working with machines, which corresponds to 95% of field capacity, in cases when allowed by the load-bearing capacity of the soil. The soil moisture was determined as per the methodology proposed by Teixeira *et al.* (2017).

In the tests, the tractor travelled for 40 m in reduced second gear with the engine at 1,750 rpm, providing an unladen travel speed of 3.51 ± 0.04 km h^{-1}. Each experimental unit was 40 m long by 3 m wide, giving a total of 120 m^2. The experimental tests with the tractor were carried out on a flat track, with approximately zero slope and a deformable surface.

The drawbar loads of the test tractor were varied by changing the gears and rotation of the braking tractor to obtain tyre slip levels up to almost 35%. When the tractor was not subjected to any load on the drawbar, wheel slip was considered to be zero, as per standard S296.4 (Asae, 1998). Drawbar force and wheel slip were determined when the tractor was moving. The tractor under test travelled with the differential lock engaged.

The tractive force on the drawbar was determined using an Omega model 'S' load cell with a capacity of 50 kN connected to a data display. The number of turns of the tractor wheels used to determine slip was established using inductive sensors and sprocket wheels, which generate pulses in the front and rear wheels when they are 4 mm apart, as described in Souza *et al*. (2022a).

A model SC-60 mechanical penetrograph was used to determine the soil cone index (Asabe, 2006b) of each plot down to a depth of 15 cm, resulting in the indices shown in Table 4.

The displacement speed was obtained applying Equation 24. Wheel slip was determined by dividing the number of revolutions of the wheel of the unladen tractor and when the tractor was in operation (Equation 25).

$$v = \frac{\Delta L}{\Delta t} \quad (24)$$

$$s = 100\left(1 - \frac{\eta_0}{\eta_1}\right) \quad (25)$$

where: ΔL - distance travelled in the experimental unit, m; Δt - time elapsed in the experimental unit, s; s - tractor wheel slip, %; η_0 - number of revolutions of the drive wheels operating with no load, dimensionless; η_1 - number of revolutions of the drive wheels when working, dimensionless.

Table 3 - Pressure settings (kPa) used in the front and rear tyres, for each type of construction

Position of the wheels	High pressure	Low pressure
	Bias tyre	
Front	221	110
Back	179	97
	Radial tyre	
Front	166	110
Back	159	97

Table 4 - Average soil cone index of the experimental plots by treatment

Treatment	In front of the front wheelset	In front of the back wheelset
	0.06 $m^3 m^{-3}$	
TM95 GP	783.4	921.0
TM95 SP	760.7	894.3
TM700 GP	762.6	896.6
TM700 SP	750.0	881.8
	0.51 $m^3 m^{-3}$	
TM700 GP	624.9	694.4
TM700 SP	615.8	684.3
TM95 GP	634.6	699.1
TM95 SP	618.8	687.7

Data analysis and the computational model

The data on front and rear wheel slip and tractive force were submitted to regression analysis, the models being selected based on the significance of the F-test, the highest coefficient of determination, and by studying the phenomenon. A probability of 5% was adopted for each analysis.

The comparisons between the experimental data and those obtained using the software were made employing the method of model identification proposed by Leite and Oliveira (2002), as described in Souza *et al.* (2022b). A probability of 5% was adopted for each analysis.

RESULTS AND DISCUSSION

Experimental data obtained from the field tests

Figure 1 shows the ratio between the values for front and rear wheel slip (λ) on dry soil. Front wheel slip increased linearly with the increase in rear wheel slip, the ratio between them varying with the operational conditions of the test. The ratio was greater when using bias tyres at the higher inflation pressure than at the lower pressure. On the other hand, when equipped with radial tyres, the values for the slip ratio were similar.

Figure 2 shows the drawbar force as a function of the ratio between the front and rear wheel slip of the tractor on dry soil. For the bias tyre, the greatest forces were seen with a λ of 1.09 at the higher pressure and 1.03 at the lower, while for the radial tyre, λ was 1.05 at the higher pressure and 1.07 at the lower. This shows that both the tyre and the inflation pressure change the value of λ that affords the maximum tractive force. This result is in line with Oiole *et al*. (2019), who consider that tractor wheel slip is a determining factor in tractive capacity, and can be related to the force required to move the implements.

It can be seen that front wheel slip increased linearly with the increase in rear wheel slip (Figure 3), also when the tractor was travelling on wet soil, with the value of the ratio (λ) between the two differing for

Figure 1 - Ratio between front and rear wheel slip (λ, Eq. 15) using bias tyres (TM95) and radial tyres (TM700+TM200) at the suggested pressure (SP) and greater than the suggested pressure (GP), for a soil moisture content of 0.06 $m^3 m^{-3}$

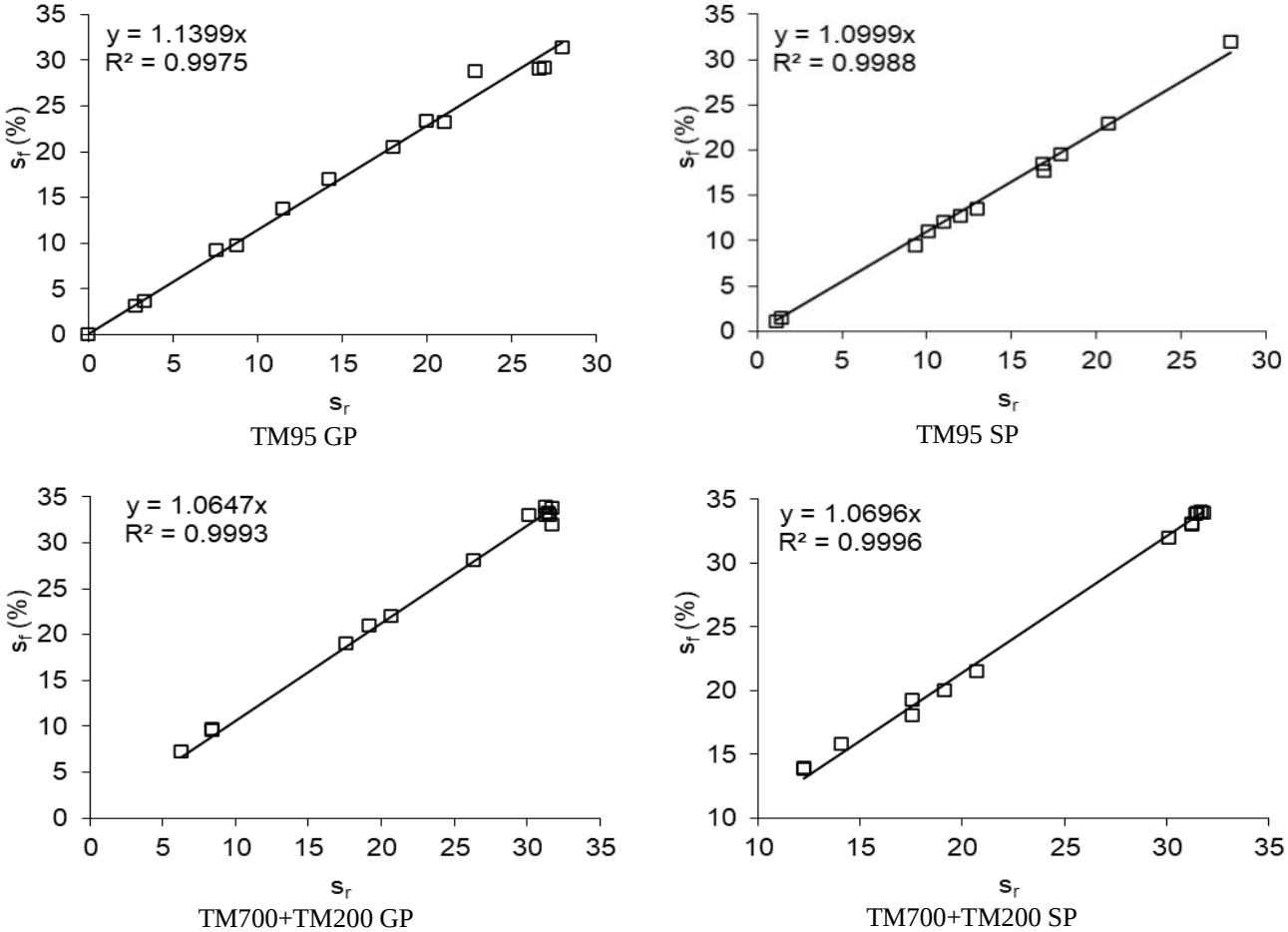

the operational conditions under test. Using bias tyres at the higher inflation pressure, the ratio was greater than at the lower pressure. When equipped with radial tyres, the values for the slip ratio were close, reflecting the same behaviour as seen for dry soil. This shows that the slip ratio between the front and rear wheels indicates a variation in the rolling radius of the tyres, and that this depends on the type of tyre and the air pressure, since according to Equation 15, the other factors involved in calculating λ are the transmission ratios, which are practically constant for the same engine acceleration.

Figure 4 shows that for the bias tyres, the greatest forces were seen with a λ of 1.06 at the higher pressure, and 1.02 at the lower, while for the radial tyres the λ was 1.02 at the higher pressure and 1.03 at the lower. Compared to the data from the dry soil, the wet soil showed lower values for λ in each of the treatments under test.

The only difference between the two soil conditions is that when wet, the soil deforms more than when dry, which can lead to a variation in tyre deformation, resulting in changes to the rolling radius of the tyre and its contact area with the surface. The forces and torques exerted by the soil on the wheel can be determined by integrating the stresses distributed along the soil-wheel interface (Jia; Smith; Peng, 2012). The variation in rolling radius seen in this study can occur for a number of reasons, including dynamic weight distribution on the axles, internal tyre pressure, wear, and specific wheel characteristics.

Test of the software

Figure 5 shows the experimental and simulated drawbar force developed by the traction devices tested for a soil moisture content of 0.06 $m^3 m^{-3}$, as a function of rear wheel slip. The model was able to simulate maximum slip values close to those obtained in the field experiment, with a mean relative error of 3.79%, while for the maximum tractive forces, the relative error was 5.76%.

Figure 2 - Drawbar force as a function of ratio between front and rear wheel slip using bias tyres (TM95) and radial tyres (TM700+TM200) at the suggested pressure (SP) and greater than the suggested pressure (GP), for a soil moisture content of 0.06 $m^3 m^{-3}$

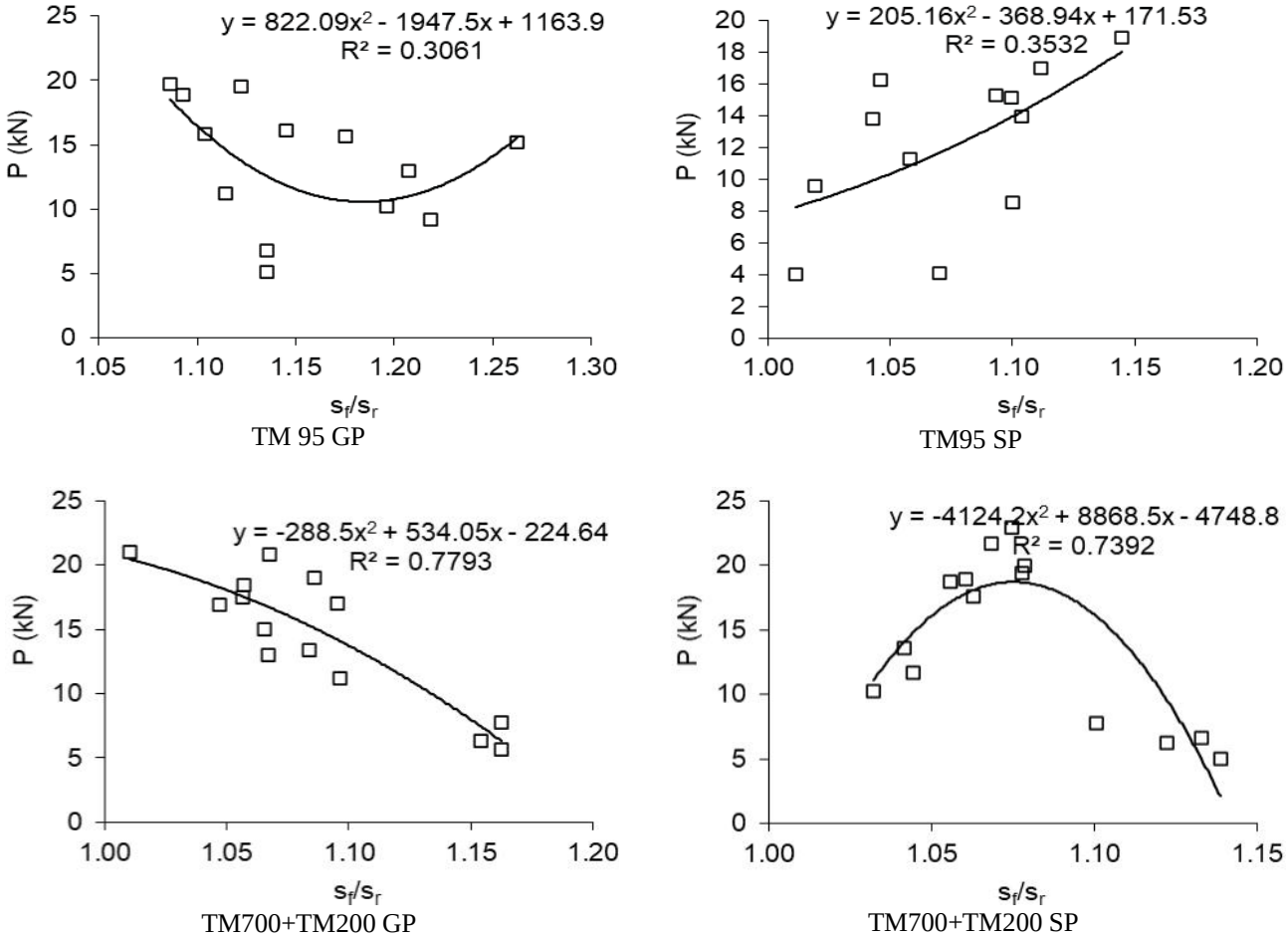

Figure 3 - Ratio between front and rear wheel slip using bias tyres (TM95) and radial tyres (TM700+TM200) at the suggested pressure (SP) and greater than the suggested pressure (GP), for a soil moisture content of 0.51 $m^3 m^{-3}$

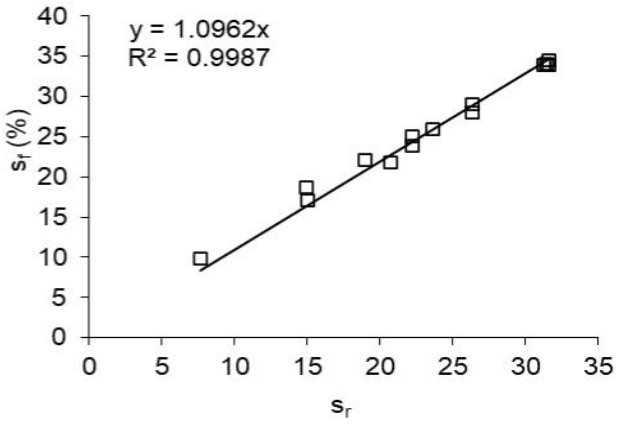

TM 95 GP

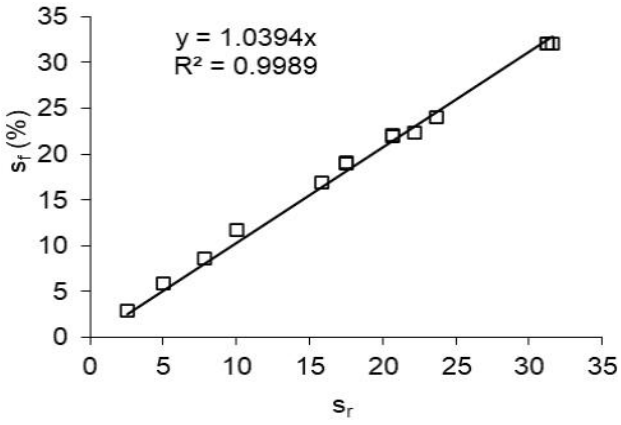

TM95 SP

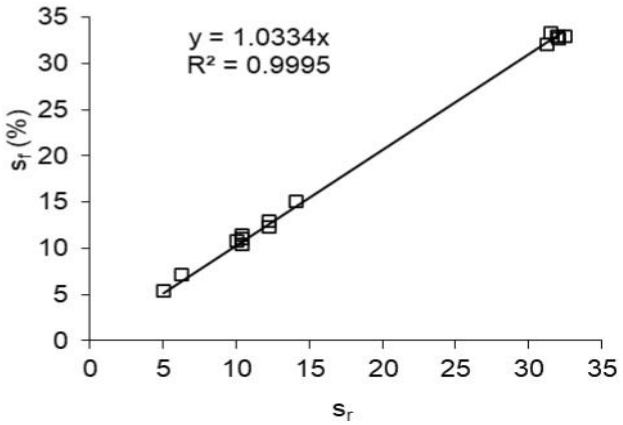

TM700+TM200 GP

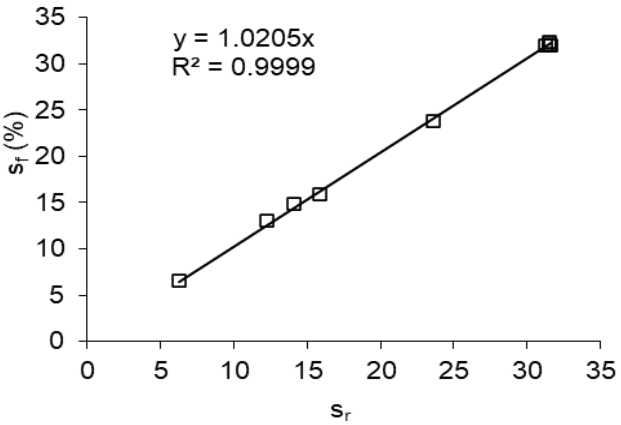

TM700+TM200 SP

Figure 4 - Drawbar force as a function of ratio between front and rear wheel slip using bias tyres (TM95) and radial tyres (TM700+TM200) at the suggested pressure (SP) and greater than the suggested pressure (GP), for a soil moisture content of 0.51 $m^3 m^{-3}$

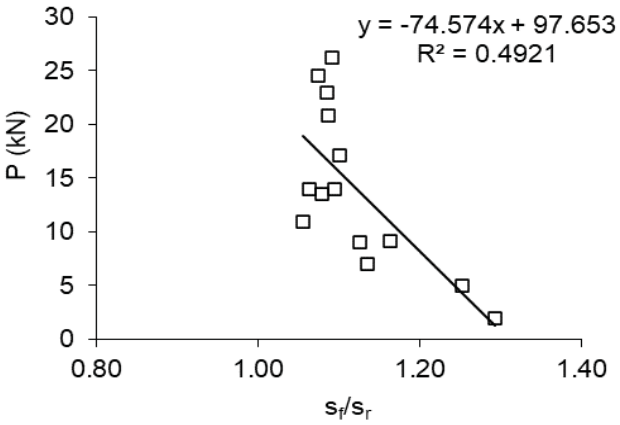

TM95 GP

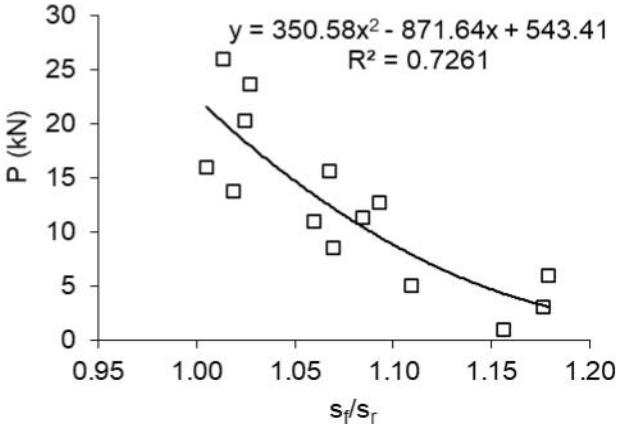

TM95 SP

Continuation Figure 4

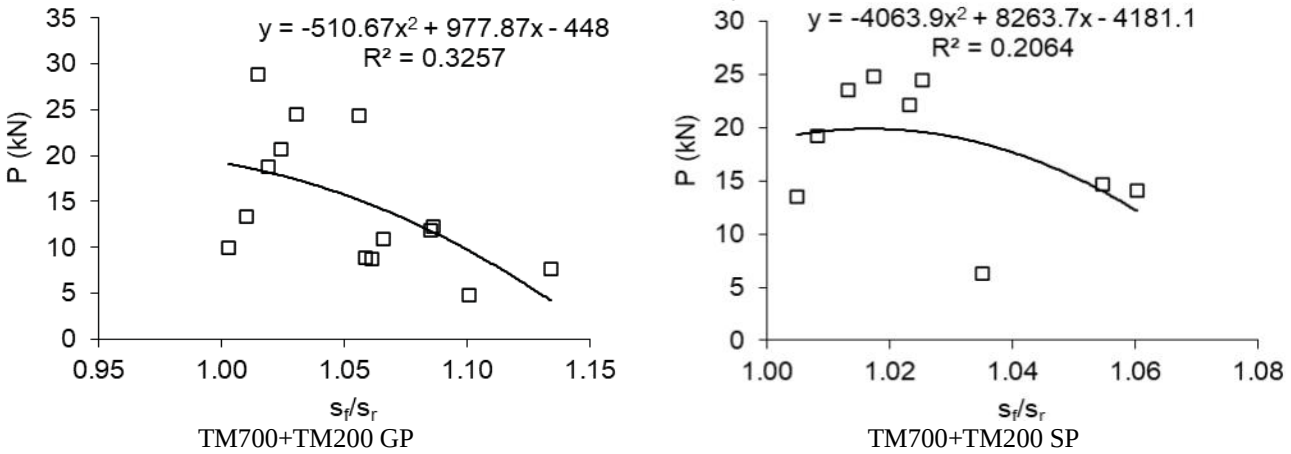

TM700+TM200 GP TM700+TM200 SP

Figure 5 - Experimental and estimated drawbar force (*P*) as a function of rear wheel slip (s_r), developed by the traction devices under a soil moisture content of 0.06 m^3 m^{-3}, for bias tyres at the lower (SP) and higher pressure (GP), and radial tyres at the lower (SP) and higher pressure (GP)

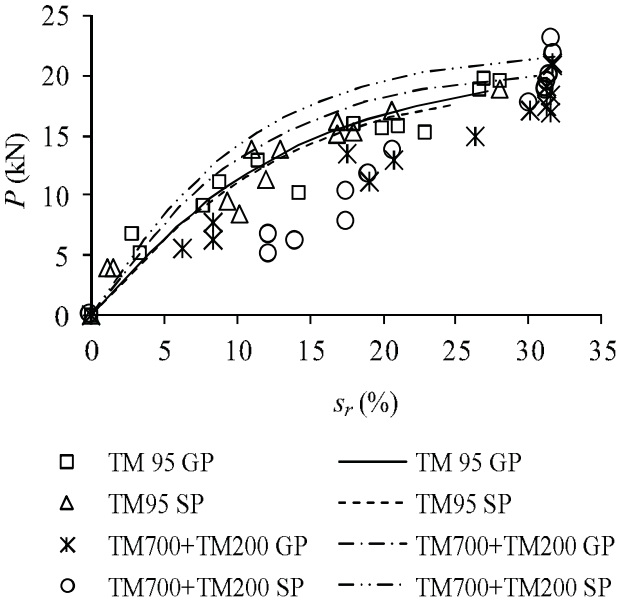

Table 6 shows the data obtained for the adjustment factor and in the identification analysis of the experimental and estimated models of drawbar force and rear wheel slip, for a soil moisture content of 0.06 m^3 m^{-3}. The values obtained for the adjustment factor (K) were lower than 0.70 for the bias tyres, whereas for the radial tyres they were greater than 0.71, showing that the proposed model requires various adjustments to fit the modelled values to the experimental values. The adjustment factor was important in matching the drawbar forces to the maximum wheel slip, however the intermediate simulated values were greater than the experimental data.

The software was able to predict simulated drawbar force with similar behaviour to the field data ($F(H_0)$), however the mean error t-test shows that the results can be considered equal to those of the experimental data only when radial tyres were used at the lower pressure (Table 6).

Table 6 shows the parameters of the comparisons between the simulated and experimental data for rear wheel slip. As in the case of tractive force when analysing the $F(H_0)$ test, all the simulated wheel slip data show similar behaviour to the experimental data. When analysing the mean error t-test, it can be seen that only the bias tyres show similar simulated and experimental data.

Figure 6 shows experimental and simulated drawbar force as a function of the rear wheel slip developed by the traction devices tested at a soil moisture content of 0.51 m^3 m^{-3}. The software was able to simulate maximum wheel slip close to that obtained in the field experiment, with a mean relative error of 1.53%, while for the maximum drawbar forces the error was 6.93%. It can be seen that the simulated values were higher than the experimental values for wheel slip rates between the minimum and maximum values obtained in the field.

Table 7 shows the data obtained for the adjustment factor and identification analysis of the experimental and estimated models for drawbar force and rear wheel slip under a soil moisture content of 0.51 m^3 m^{-3}. The values for the adjustment factor (Equations 11 and 12) obtained for wet soil (Table 7) were higher than those seen for dry soil (Table 6). This shows that there is less need to calibrate the proposed model based on the D497.5 standard (Asabe, 2006a) when simulating traction in a dystrophic Red-Yellow Argisol close to field capacity than when excessively dry.

Table 6 - Comparative analysis between the models for drawbar force and rear wheel slip on dry ground for bias tyres at the lower (SP) and higher pressure (GP), and radial tyres at the lower (SP) and higher pressure (GP), for a soil moisture content of 0.06 $m^3 m^{-3}$

Factor for analysis	TM 95 GP	TM95 SP	TM700+TM200 GP	TM700+TM200 SP
Adjustment factor (K)	0.70	0.67	0.71	0.75
		Drawbar force		
F(H0)	0.558^{ns}	0.213^{ns}	0.264^{ns}	0.145^{ns}
Standard error t-test	7.003*	2.308*	4.444*	1.521^{ns}
$r_{Yj}Y_1 \geq \lvert 1-\dot{e}\rvert$?	Yes	Yes	Yes	Yes
		Rear wheel slip		
F(H0)	0.007^{ns}	0.023^{ns}	0.004^{ns}	0.017^{ns}
Standard error t-test	1.450^{ns}	0.572^{ns}	10.278*	10.075*
$r_{Yj}Y_1 \geq \lvert 1-\dot{e}\rvert$?	Yes	Yes	Yes	Yes

^{ns} - not significant, * - significant at 5% probability

Figure 6 - Experimental and estimated drawbar force (P) as a function of rear wheel slip (sr) developed by the traction devices under a soil moisture content of 0.51 $m^3 m^{-3}$, for bias tyres at the lower (SP) and higher pressure (GP), and radial tyres at the lower (SP) and higher pressure (GP)

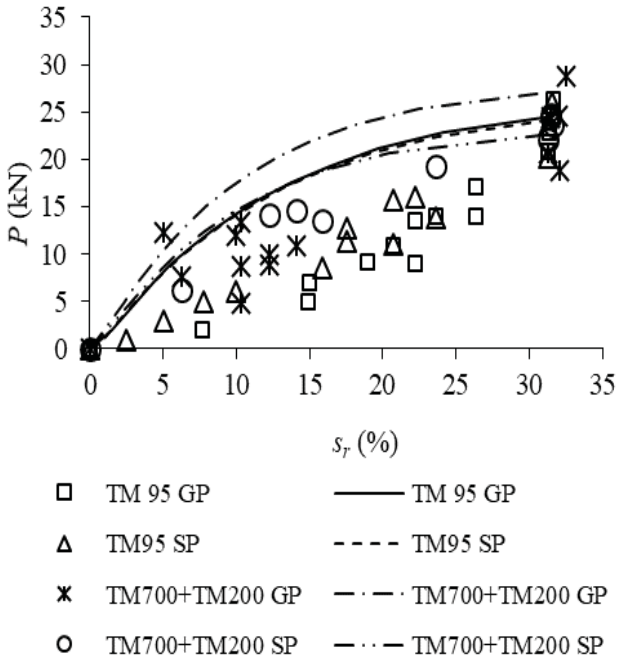

The simulated drawbar force shows similar behaviour to the field data [$F(H_0)$] for the experimental drawbar force; however, analysing the mean error t-test, it can be seen that only where the bias tyres were used at the lower pressure can the simulated data be considered equal to the experimental data.

Analysing the parameters of the comparisons between the simulated and experimental data for rear wheel slip, which are shown in Table 7, what happened to tractive force when analysing the $F(H_0)$ test also happened to all the simulated wheel slip data, showing similar behaviour to the experimental data. However, analysing the error t-test, only the simulated data for the radial tyres at the higher pressure were similar to the experimental data.

Results obtained by Hu *et al.* (2021) show that the proposed model for representing the soil-wheel interaction with curves and slippage maintained a good fit with the analytical model, validating the efficiency of the modelling and the method used for calibrating the parameters. For Damanauskas and Janulevičius (2015), tyre pressure and wheel loads are easily managed parameters that play a significant role in controlling the slippage, fuel consumption and field performance of a tractor. In this case, the model presented in this study could be updated to better adjust the relationship between tractive force and wheel slip.

Table 7 - Comparative analysis between drawbar force and rear wheel slip obtained on dry soil for bias tyres at the lower pressure (SP) and higher pressure (GP), and radial tyres at the lower (SP) and higher pressure (GP), for a soil moisture content of 0.51 $m^3 m^{-3}$

Factor for analysis	TM95 GP	TM95 SP	TM700+TM200 GP	TM700+TM200 SP
Adjustment factor (K)	0.91	0.88	0.98	0.81
		Drawbar force		
F(H0)	0.143^{ns}	0.094^{ns}	0.033^{ns}	0.179^{ns}
Standard error t-test	2.374*	0.363^{ns}	2.317*	5.172*
$r_{Yj}Y_1 \geq \lvert 1-\dot{e}\rvert$?	Yes	Yes	Yes	Yes

Continuation Table 7

		Rear wheel slip		
F(H0)	0.050^{ns}	0.013^{ns}	0.002^{ns}	0.008^{ns}
Standard error t-test	8.852*	8.993*	3.031^{ns}	6.803*
$r_{Y_j}Y_1 \geq \lvert 1-e \rvert$?	Yes	Yes	Yes	Yes

^{ns} - not significant, * - significant at 5% probability

CONCLUSIONS

1. On both extremely dry soil and soil with a high level of moisture, when using bias tyres at the lower inflation pressure, the ratio between front and rear wheel slip was lower than at the higher pressure, whereas when equipped with radial tyres, the slip ratios were similar, indicating the same variation in tyre rolling radius for each type of tyre and selected air pressure;
2. With the bias tyres, the greatest drawbar forces occur for a front and rear wheel slip ratio of 1.09 at the higher pressure and 1.03 at the lower, while for the radial tyres this ratio was 1.05 at the higher pressure and 1.07 at the lower, demonstrating that both the type of tyre and the inflation pressure alter the value of the wheel slip ratio to provide maximum tractive force;
3. Computer software was successfully developed to calculate the data for the proposed model. Using the software, it is possible to estimate the tractive behaviour of a tyre tractor with auxiliary front wheel drive. However, the tractive force was overestimated for the same amount of wheel slip; this needs to be corrected if the model is to be used directly in the field.

ACKNOWLEDGMENTS

The authors thank the Brazilian Federal Agency for the Support and Evaluation of Graduate Education (CAPES) for the financial support to conduct and disseminate this research (AFP-123-2023/PROAP/CAPES-UFGD). The authors also thank to the Federal University of Viçosa, for providing the experimental field and the sensors. The lead author thanks the CAPES for the grant awarded.

REFERENCES

ALMEIDA, R. A. S. de; TAVARES-SILVA, C. A.; SILVA, S. de L. Desempenho energético de um conjunto trator-semeadora em função do escalonamento de marchas e rotações do motor. **Revista Agrarian**, v. 3, n. 7, p. 63-70, 2010.

ARAUJO, A. L. F. *et al.* The use of modelling to determine the limiting conditions for resuming soil loading by tractor in an area of sugar cane under reduced tillage. **International Journal for Innovation Education and Research**, v. 10, p. 172-188, 2022. DOI: http://dx.doi.org/10.31686/ijier.vol10.iss11.3801.

ASABE. Agricultural machinery management data. **ASAE Standard D497.5**. St. Joseph, 2006a. p. 391-398.

ASABE. Soil cone penetrometer. **ASAE Standard S313.3**. St. Joseph, 2006b. p. 903-904.

ASAE. General terminology for traction of agricultural tractors, self-propelled implements, and traction and transport devices. **ASAE Standard S296.4**. St. Joseph: ASAE, 1998. p. 118-120.

AUBERT, B. A.; SCHROEDER, A.; GRIMAUDO, J. It as enabler of sustainable farming: an empirical analysis of farmer's adoption decision of precision agriculture technology. **Decision Support Systems**, v. 54, n. 1, p. 510-520, 2012.

BORGES, P. H. M. *et al*. Estimation of fuel consumption in agricultural mechanized operations using artificial neural networks. **Engenharia Agrícola**, v. 37, p. 136-147, 2017. DOI: https://doi.org/10.1590/1809-4430-Eng.Agric.v37n1p136-147/2017.

BRIXIUS, W.W. **Traction prediction equations for bias ply tires**. St. Joseph: ASAE, 1987. 8 p.

CHAMON, J. E. **Excel com VBA na prática**. São Paulo: Editora Érica, 2019. 184 p.

DAMANAUSKAS, V.; JANULEVIČIUS, A. Differences in tractor performance parameters between single-wheel 4WD and dual-wheel 2WD driving systems. **Journal of Terramechanics**, v. 60, p. 63-73, 2015.

FAVERO, L. P. L.; BELFIORE, P. P. **Manual de análise de dados: estatística e modelagem multivariada com Excel®, SPSS® e Stata®**. Rio de Janeiro: Elsevier, 2017. 1187 p.

GOERING, C. E. *et al.* **Off-road vehicle engineering principles**. St. Joseph: ASAE, 2003. 474 p.

HART, L.; QUENDLER, E.; UMSTAETTER, C. Sociotechnological sustainability in pasture management: labor input and optimization potential of smart tools to measure herbage mass and quality. **Sustainability**, v. 14, n. 12, e.7490, 2022. DOI: https://doi.org/10.3390/su14127490.

HU, C. *et al.* Analytical modeling and DEM analysis of soil-wheel interaction under cornering and skidding conditions in off-road vehicles. **AIP Advances**, v. 11, e.085122, 2021. DOI: https://doi.org/10.1063/5.0057046.

JIA, Z.; SMITH, W.; PENG, H. Terramechanics-based wheel-terrain interaction model and its applications to off-road wheeled mobile robots. **Robotica**, v. 30, n. 3, p. 491-503, 2012. DOI: https://doi.org/10.1017/S0263574711000798.

LEITE, H. G.; OLIVEIRA, F. H. T. Statistical procedure to test the identity of analytical methods. **Communications in Soil Science and Plant Analysis**, v. 33, p. 1105-1118, 2002. DOI: https://doi.org/10.1081/CSS-120003875.

OIOLE, Y. A. *et al.* Energy performance in disc harrowing operation in different gradients and gauges. **Engenharia Agrícola**, v. 39, n. 6, p. 769-775, 2019. DOI: https://doi.org/10.1590/1809-4430-Eng.Agric.v39n6p769-775/2019.

PINHO, T.; CUNHA, J. B.; MORAIS, R. Tecnologias da eletrônica e da computação na recolha e integração de dados em agricultura de precisão. **Revista de Ciências Agrárias**, v. 38, n. 3, p. 291-304, 2015.

PRON, S. *et al*. Modeling of the transport and production complex in the growing of agricultural crops, taking into account the aviation component. **Eastern-European Journal of Enterprise Technologies**, v. 2/3, n. 104, p. 30-39, 2020. DOI: https://doi.org/10.15587/1729-4061.2020.198742.

SANTOS, H. G. *et al*. **Sistema brasileiro de classificação de solos**. Brasília, DF: Embrapa, 2018. 356p. Disponível em: https://www.infoteca.cnptia.embrapa.br/infoteca/handle/doc/1094003. Acesso em: 11/07/2024.

SCHLOSSER, J. F. *et al*. Power hop in agricultural tractors. **Ciência Rural**, v. 50, n. 8, e20200199, 2020. DOI: https://doi.org/10.1590/0103-8478cr20200199.

SICHONANY, O. R. de A. O. *et al*. Telemetria na transmissão de dados de desempenho de máquinas agrícolas utilizando tecnologia GSM/GPRS e ZigBee. **Ciência Rural**, v. 42, p. 1430-1433, 2012.

SOUZA, C. M. A. de *et al.* Artificial neural networks to predict efficiencies in semi-mechanized bean (*Phaseolus vulgaris* L.) harvest. **Engenharia Agrícola**, v. 42, e20210097, 2022b. DOI: http://dx.doi.org/10.1590/1809-4430-Eng.Agric.v42nepe20210097/2022.

SOUZA, C. M. A. de *et al*. Performance of a planter-fertiliser under reduced soil preparation: furrowers, speeds and depths when sowing maize. **Revista Ciência Agronômica**, v. 53, e20207476, 2022a. DOI: http://doi.org/10.5935/1806-6690.20220014.

TEIXEIRA, P. C. *et al*. **Manual de métodos de análise de solo**. Brasília, DF: Embrapa, 2017. 574 p.

ZHANG, C.; KOVACS, J. M. The application of small unmanned aerial systems for precision agriculture: a review. **Precision Agriculture**, v. 13, n. 6, p. 693-712, 2012.

ZHANG, X.; SEELAN, S.; SEIELSTAD, G. Digital Northern Great Plains: a web-based system delivering near real time remote sensing data for precision agriculture. **Remote Sensing**, v. 2, n. 3, p. 861-873, 2010.